

RESEARCH LETTER

10.1002/2015GL065957

Key Points:

- Wind-driven Beaufort Gyre dynamics is simulated within an eddy-resolving model
- Mesoscale eddies play a key role in constraining variations in freshwater content
- The Beaufort Gyre is currently at its highest sensitivity to wind stress forcing

Correspondence to:

G. E. Manucharyan,
gmanuch@caltech.edu

Citation:

Manucharyan, G. E., and M. A. Spall (2016), Wind-driven freshwater buildup and release in the Beaufort Gyre constrained by mesoscale eddies, *Geophys. Res. Lett.*, *43*, 273–282, doi:10.1002/2015GL065957.

Received 27 AUG 2015

Accepted 1 OCT 2015

Accepted article online 5 OCT 2015

Published online 6 JAN 2016

Wind-driven freshwater buildup and release in the Beaufort Gyre constrained by mesoscale eddies

Georgy E. Manucharyan¹ and Michael A. Spall¹¹Department of Physical Oceanography, Woods Hole Oceanographic Institution, Woods Hole, Massachusetts, USA

Abstract Recently, the Beaufort Gyre has accumulated over 20,000 km³ of freshwater in response to strong anticyclonic atmospheric winds that have prevailed over the gyre for almost two decades. Here we explore key physical processes affecting the accumulation and release of freshwater within an idealized eddy-resolving model of the Beaufort Gyre. We demonstrate that a realistic halocline can be achieved when its deepening tendency due to Ekman pumping is counteracted by the cumulative action of mesoscale eddies. Based on this balance, we derive analytical scalings for the depth of the halocline and its spin-up time scale and emphasize their explicit dependence on eddy dynamics. Our study further suggests that the Beaufort Gyre is currently in a state of high sensitivity to atmospheric winds. However, an intensification of surface stress would inevitably lead to a saturation of the freshwater content—a constraint inherently set by the intricacies of the mesoscale eddy dynamics.

1. Introduction

The Arctic Ocean is an essential part of our changing climate system [Moritz *et al.*, 2002]. Because it is strongly affected by atmospheric dynamics, radiative processes, and is interconnected with both the Pacific and Atlantic Oceans, the Arctic maintains a complex circulation balancing heat and salt budgets. Time dependence in forcing can lead to a strong response in sea ice cover [Eisenman and Wettlaufer, 2009; Boé *et al.*, 2009; Schweiger *et al.*, 2011; Krishfield *et al.*, 2014], circulation patterns [Dickson *et al.*, 2000; Morison *et al.*, 2012; McPhee, 2013], CO₂ uptake [Cai *et al.*, 2010], and biomass production [Tremblay *et al.*, 2011; McLaughlin and Carmack, 2010; Li *et al.*, 2009]. Here we bring the reader's attention to the freshwater content that has been increasing primarily in the Beaufort Gyre [Rabe *et al.*, 2011, 2014; Haine *et al.*, 2015]—a major anticyclonic circulation in the upper 300 m of the Canada Basin in the Arctic Ocean [Aagaard and Carmack, 1989; Proshutinsky *et al.*, 2002].

The surface freshwater provides a stratification cap preventing deep but warm Atlantic waters from reaching the surface and melting the sea ice. Furthermore, excessive freshwater can propagate from the Arctic to the North Atlantic Ocean and potentially affect the formation of deep water masses—an important component of the Meridional Overturning Circulation. It has also been hypothesized that freshwater from the Arctic might have contributed to Great Salinity Anomalies [Dickson *et al.*, 1988; Belkin *et al.*, 1998; Belkin, 2004] with potential consequences for the global climate [Häkkinen, 1999; Zhang and Vallis, 2006]. Nonetheless, a quantitative understanding of the gyre's freshwater accumulation and release is not well developed.

Observational and modeling studies identify the importance of primarily anticyclonic (clockwise) surface stress (Figure 1) as a forcing for the gyre [Proshutinsky and Johnson, 1997; Proshutinsky *et al.*, 2002, 2009; Timmermans *et al.*, 2011; Watanabe, 2013] which can change to weakly cyclonic regimes and affect the gyre circulation [Proshutinsky and Johnson, 1997; Proshutinsky *et al.*, 2002]. The converging Ekman flow associated with the anticyclonic atmospheric stress advects relatively fresh surface waters from the boundaries and pumps them into the interior of the gyre, thus deepening the halocline (a region of sharp vertical gradient in salinity) and increasing the freshwater content (FWC) of the gyre. However, the accumulation of freshwater under steady surface stress forcing cannot last indefinitely, and a steady state gyre can only be achieved if there is a process opposing this freshwater pumping.

Here we point to the cumulative action of mesoscale eddies as a major mechanism that counteracts the halocline deepening due to Ekman pumping. Because the halocline is shallower near the coastal boundaries and deepens toward the interior, the gyre not only holds FWC but also contains a large amount of gravitational

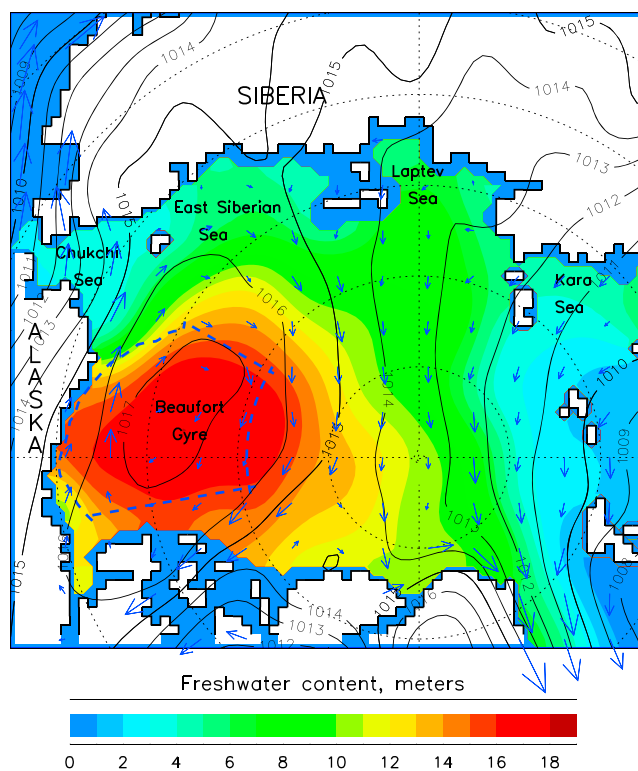


Figure 1. Representative conditions of the Arctic Ocean. Colors: freshwater content averaged from a compilation of in situ observations over the period of 2000–2009. Black contours: sea level pressure obtained from National Centers for Environmental Prediction reanalysis for the same period. Arrows: geostrophic winds calculated based on the sea level pressure. Note the presence of anticyclonic atmospheric winds surrounding a region of maximum freshwater content. Figure courtesy of A. Proshutinsky.

potential energy. Analogous to many other regions of the World Ocean, this potential energy can be released through the process of baroclinic instability accompanied by the generation of mesoscale eddies [Pedlosky, 1982; Vallis, 2006]. Cumulatively, these eddies act to flatten the halocline [Marshall and Radko, 2003; Karsten et al., 2002] thus constraining its deepening and setting its bulk properties [Marshall et al., 2002].

Observations in the Arctic Ocean reveal that it is populated with mesoscale eddies [Manley and Hunkins, 1985; Timmermans et al., 2008; Dmitrenko et al., 2008; Watanabe, 2011; Zhao et al., 2014] with studies suggesting that the origins of such eddies are the instabilities of the oceanic fronts [Manucharyan and Timmermans, 2013] and boundary currents [Watanabe, 2013; Spall et al., 2008; Spall, 2013]—all associated with the release of the accumulated gravitational potential energy. Nonetheless, despite mesoscale eddies being ubiquitously observed in the Beaufort Gyre, their cumulative influence on its freshwater balance has not been clearly established.

Here we investigate the major physical processes that govern the accumulation and release of freshwater in the Beaufort Gyre. We illustrate our discussions using an observationally consistent conceptual model of the gyre that explicitly resolves mesoscale eddies.

2. Beaufort Gyre Model

2.1. Formulation

We focus on the internal gyre dynamics and apply an idealized modeling approach combined with analytical investigations. We model the Beaufort Gyre in a closed circular basin with a radius of 600 km representing an area with the observed maximum in Arctic FWC (Figure 1). Because the water mass exchanges with the Pacific and Atlantic Oceans primarily occur through topographically trapped boundary currents [Rudels, 2012; Aksenov et al., 2011], we parameterize them by restoring salinity at the boundaries to a representative vertical profile. This near-coastal salinity distribution is set by a complex interplay between strongly variable inflows of both fresh and salty waters affected by intermittent wind-driven coastal upwelling [Pickart et al., 2013]—processes which we do not attempt to model here. Instead, consistent with observations, we impose a typical salinity profile at the boundaries which consists of a fresher upper layer of about 50 m thickness (salinity of 29) and salty waters beneath (bottom salinity 34). While there are indications of decadal variability of river outflows [Peterson et al., 2002] and changes in Atlantic and Pacific water inflow [Bourgain and Gascard, 2012], we consider these processes (as well as changes in sea ice [Krishfield et al., 2014]) to be secondary to the basic wind-driven dynamics of the gyre. We note, however, that these processes can significantly affect the temporal and spacial variability of the gyre. Nonetheless, for simplicity, we keep the coastal salinity profile constant in time and allow the interior of the gyre to naturally draw a necessary amount of fresh/salty waters from its boundaries as is required to satisfy its wind-driven adjustment.

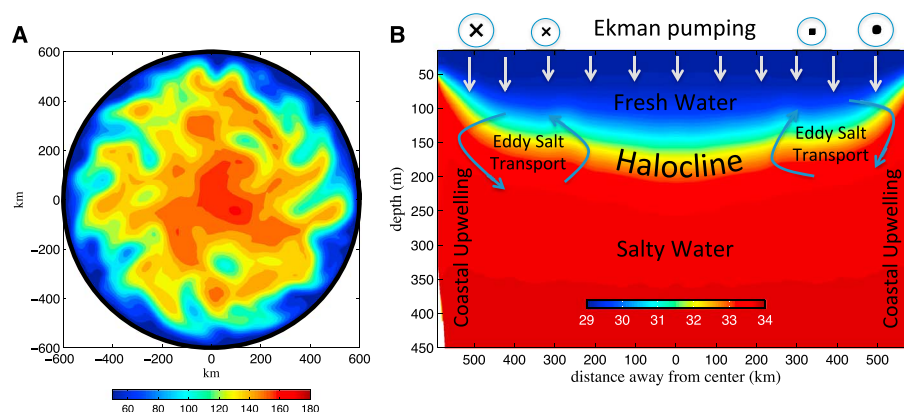


Figure 2. (a) Instantaneous field of halocline depth (in meters) for the equilibrated gyre state numerically simulated for a reference surface stress ($\tau_0 = 0.015 \text{ N m}^{-2}$). Note the presence of radial gradients in halocline depth and a pronounced eddy field. (b) Azimuthally averaged salinity distribution (in color). Overimposed is a schematic view of the gyre features: wind-driven Ekman pumping at the surface, opposing eddy-driven circulation (arrows), and the resulting halocline layer that is deeper in the interior. Note that the model domain extends to 900 m depth, but here salinity field is shown only down to 450 m below which the isopycnals are almost flat.

We force the gyre via the idealized anticyclonic surface stress with the fluid dynamical and salt transport processes simulated in an eddy-resolving configuration of the Massachusetts Institute of Technology general circulation model (MITgcm), described in more detail in Appendix A. We do not attempt to simulate the sea ice distribution and assume here that it evolves largely independent of the halocline dynamics and can thus be considered as an external factor. Nonetheless, atmosphere-ocean momentum transfer is modified by the presence of the sea ice [Martin *et al.*, 2014; Davis *et al.*, 2014]—an issue that we address by exploring gyre’s sensitivity to a wide range of surface stress forcing $\tau \in [0.002, 0.15] \text{ N m}^{-2}$.

To put this range in perspective, consider the following estimates. Timmermans *et al.* [2014] used sea ice drift data to estimate a representative value of Ekman pumping of 2 cm d^{-1} , corresponding to a wind stress in our model of 0.01 N m^{-2} . Martin *et al.* [2014] estimated a basin average surface stress value of 0.05 N m^{-2} , although only a portion of it would contribute to Ekman pumping. We note that these stress estimates use an ice-ocean drag coefficient that is poorly constrained by observations [Cole *et al.*, 2014]. For an ice-free Arctic Ocean scaling estimates using air-ocean drag coefficient of 0.002 and atmospheric winds of $U = 8 \text{ m s}^{-1}$ would lead to the strongest stress that we used in our simulations ($\tau = 0.15 \text{ N m}^{-2}$); our lower bound corresponds to virtually negligible atmospheric winds. Throughout the manuscript, we consider surface stress of $\tau = 0.015 \text{ N m}^{-2}$ as a representative case for present-day Beaufort Gyre.

2.2. Simulations of the Gyre Response to Surface Stress

The model presented here is designed to investigate the core features of the Beaufort Gyre, in particular the halocline depth and its response to changes in surface stress. At any particular point in time the gyre is populated with mesoscale eddies that exist within a persistent large-scale gradient in halocline depth (Figure 2). On average, the model halocline driven by a representative surface stress magnitude of $\tau = 0.015 \text{ N m}^{-2}$ is shallow at the boundaries at 50 m and reaches a depth of about 150 m in the interior (Figure 2b). A salinity difference of about 5 across the tilted halocline supports an anticyclonic circulation of about 0.15 m s^{-1} near the coastal boundaries—source regions for eddy and water mass production.

The model gyre holds a total freshwater volume of about $16,000 \text{ km}^3$ with a maximum local FWC reaching 20 m in the center of the gyre (FWC is calculated by vertically integrating the salinity referenced to bottom salinity of 34 from the surface to 350 m where the isopycnals are nearly flat). This simulated value of FWC generally agrees with observationally based estimates in the range of 19–24 m [Proshutinsky *et al.*, 2009; Haine *et al.*, 2015], although we note that the model does not include a contribution from a relatively fresh surface mixed layer. Thus, this key feature of the gyre driven by a representative constant surface stress is qualitatively and to a large degree quantitatively consistent with observations.

We have run the numerical model to statistical equilibrium for a series of different surface stress forcing. The FWC is close to the boundary value of 8 m for very weak stress (corresponding to a flat halocline) but increases

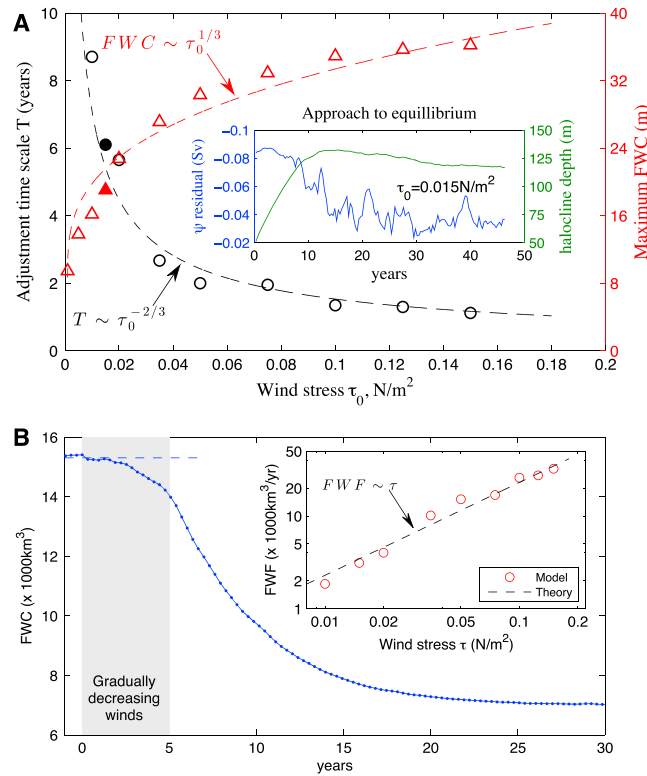


Figure 3. (a) The dependence of the maximum steady Beaufort Gyre FWC (red) and its e -folding spin-up time scale (black) on surface stress as simulated by the eddy-resolving model. Dashed lines show theoretical scaling as in equations (2) and (3). Inset shows the gyre spin-up process ($\tau = 0.015$ N m⁻²) with a deepening of the basin-averaged halocline depth (green) and a weakening of residual circulation $\tilde{\psi}$ (blue) (see Appendix B). (b) Time evolution of freshwater content (blue) for a numerical experiment with decreasing surface stress. Inset shows maximum freshwater flux (red circles) that a gyre, initially at equilibrium under surface stress forcing τ , releases after the winds have been turned off; dashed line shows analytical scaling (equation (4)).

rapidly with increasing winds and saturates at approximately 34 m for very strong winds (Figure 3a, red). The e -folding time also shows strong sensitivity to surface stress with rapid adjustment times for strong winds and slow adjustment times for weak winds (Figure 3a, black). These results clearly show that the halocline properties strongly depend on the mean surface stress. To interpret this sensitivity, we now consider the dynamics of such a wind-forced circulation.

3. The Role of Mesoscale Eddies

Following a transform Eulerian mean framework [e.g., Vallis, 2006], a key balance for the statistically equilibrated gyre can be comprehensively illustrated from the point of view of its salt budget.

The advection by mean currents and eddy-driven salt transport provide dominant contributions to the salt balance of the gyre [Marshall and Radko, 2003; Henning and Vallis, 2005; Su et al., 2014]. The Eulerian overturning circulation, $\tilde{\psi}$, is driven by the Ekman pumping that deepens the halocline, increasing the potential energy of the ocean. This potential energy is being continuously released via instabilities that generate deformation-scale eddies evident in the instantaneous field of halocline depth (Figure 2a).

When eddy salt fluxes are aligned with isopycnals (adiabatic limit), their effects can be represented with an eddy stream function, ψ^* , that acts to flatten the halocline and can be defined as

$$\psi^* = -\frac{\overline{v'b'}}{b_z} \quad (1)$$

where $\overline{v'b'}$ is the average radial eddy buoyancy flux and b_z is the average vertical buoyancy gradient [Marshall and Radko, 2003; McIntosh and McDougall, 1996; Birner, 2010]. The residual between the two opposing circulations, $\tilde{\psi} = \tilde{\psi} + \psi^*$, drives changes in the halocline depth.

After initial adjustment, the eddy-resolving numerical model achieves a steady state when $\tilde{\psi} \approx 0$ (Figure 3a, inset) implying that the Eulerian mean transport has to a large degree been compensated by eddy transport. We note, however, that the residual stream function $\tilde{\psi}$ does not completely approach zero in the numerical model because of the vertical diffusion (an upper estimate for the Arctic Ocean of $\kappa_v = 10^{-5}$ m² s⁻¹ was used in the model). Indeed, following Nikurashin and Vallis [2011] and Karsten and Marshall [2002], a nondimensional diffusiveness number $\epsilon = \frac{\rho_0 f \kappa_v R}{\tau_0 h} \approx 0.3$ characterizes the relative effect of vertical mixing compared to vertical pumping (ρ_0 being a reference ocean density, f the Coriolis parameter, R the gyre radius, and h the halocline depth). The diffusiveness is not large for this case but becomes increasingly important for weaker winds or stronger mixing.

In the limit of absent Ekman pumping, the purely boundary-forced configuration as was used by Spall [2013] implies that the eddy fluxes of fresh and salty water from the boundaries should be entirely balanced by vertical diffusion in the interior of the gyre. However, for relatively strong anticyclonic winds ($\tau > \sim 0.01 \text{ N m}^{-2}$) the wind-driven Ekman salt transport is primarily balanced by eddy fluxes with vertical mixing accounting for only minor deviations from this balance. We thus continue with our analysis for cases with moderate-to-strong stress forcing where the effects of vertical mixing can be omitted.

3.1. Halocline Depth

In the interior of the gyre it is possible to construct an analytical solution for the halocline. First, the Eulerian overturning (in the (r, z) plane) is determined by the Ekman transport, $\tilde{\psi} = \tau/(\rho_0 f)$ [Marshall and Radko, 2003], where the azimuthal surface stress $\tau(r) < 0$ (anticyclonic winds) varies with the radial distance from the center of the gyre r . Second, the eddy buoyancy fluxes in the definition of eddy stream function (equation (1)) can be conventionally parameterized as $v'b' = -K\bar{b}_r$, where K is the eddy diffusivity akin to that of Gent and McWilliams [1990]. In general, the eddy diffusivity can itself be a function of the local isopycnal slope, $s = \bar{b}_r/\bar{b}_z$, with existing parameterizations suggesting different power law dependencies [Green, 1970; Visbeck et al., 1997; Jansen et al., 2015; Held and Larichev, 1996]. While strong observational support for a particular eddy parameterization scheme is not yet available for the Arctic Ocean, it appears that assuming $K \sim s^2$ gives the best agreement with our model simulations. Hence, we carry on our theoretical analysis taking $K = ks^2$ corresponding to $\psi^* = ks^3$, where k is a constant eddy efficiency coefficient.

Thus, in the adiabatic limit a statistically steady state is achieved when $\tilde{\psi} = \tau/(\rho_0 f) + ks^3 = 0$ and hence the mean slope, s , is directly related to the local stress, allowing one to obtain an expression for the halocline depth in the center of the gyre:

$$h = h_b + \int_0^R \left(\frac{-\tau}{\rho_0 f k} \right)^{\frac{1}{3}} dr, \quad (2)$$

where h_b is the depth of the halocline near the boundaries, presumably set by coastal processes, and $R \approx 600 \text{ km}$ is the gyre radius. The scaling of FWC dependence on surface stress predicted by equation (2) compares well with that found in the numerical model (Figure 3a). Note that this theory predicts the halocline depth in the interior to be related to the basin-integrated measure of surface stress—not to the local value of Ekman pumping (equation (2)) which can be very small near the center of the gyre [Timmermans et al., 2014].

Consistent with numerical simulations, the theory (equation (2)) predicts a high gyre sensitivity for weak forcing ($\tau < 0.04 \text{ N m}^{-2}$) and a reduced sensitivity (or saturation) for strong forcing (Figure 3a, red). The saturation arises due to a strong dependence of eddy diffusivity on halocline slope ($K \sim s^2$). Thus, the model suggests that the Beaufort Gyre, currently under relatively weak forcing ($\tau \sim 0.015 \text{ N m}^{-2}$), is highly sensitive to surface stress—consistent with observations of dramatic wind-forced FWC changes over the past decades [Proshutinsky et al., 2009]. We emphasize that the saturation discussed here is solely with respect to surface stress forcing and does not take into account water mass modification at the shelves as well as export and growth/melt of sea ice.

3.2. Beaufort Gyre Adjustment Time

The transient gyre dynamics can be clearly illustrated if one considers the spin-up of the halocline from an initial state at its near-boundary depth of 50 m. As soon as the winds are turned on, a strong residual circulation with magnitude over 0.08 Sv ($1 \text{ Sv} = 10^6 \text{ m}^3 \text{ s}^{-1}$), entirely due to the Ekman pumping, initially deepens the halocline in the interior (see inset of Figure 3a). The eddy field strengthens in response to the increasing halocline slope eventually reducing $\tilde{\psi}$ down to about 0.03 Sv (Figure 3a, blue curve). After the substantial reduction of the residual circulation the equilibration has largely been completed. We observe analogous dynamics for a spin-down with decreasing winds.

For present-day Arctic conditions with $\tau \approx 0.015 \text{ N m}^{-2}$ the model gyre adjusts to atmospheric winds with an e-folding time scale, T , of about 6 years (Figure 3a, inset). This time is generally consistent with idealized [Davis et al., 2014; Lique et al., 2015] and more comprehensive Arctic climate models [Condron et al., 2009; Stewart and Haine, 2013]. Such a prolonged adjustment implies that the ocean will act to integrate the impact from highly transient wind oscillations and in essence respond only to their decadal trends.

This time scale can be thought of as the time needed for Ekman pumping to deepen the halocline to its equilibrium depth such that $T \sim h/W_{Ek}$, where $W_{Ek} = \text{curl}(\tau/\rho_0 f) \sim \tau_0/(R\rho_0 f)$ is the Ekman pumping velocity.

However, T is also set by the time necessary for the eddies to propagate from the boundaries, where the salt and fresh water sources are toward the interior of the domain. Hence, T is inversely proportional to the eddy mixing coefficient K and proportional to the area of the gyre such that $T \sim R^2/K$ [Jones *et al.*, 2011; Allison *et al.*, 2011]. Note that eddy diffusivity itself depends on halocline depth as $K = ks^2 \sim k(h/R)^2$ because halocline slope $s \sim h/R$. Equating the advective and eddy mixing time scales not only allows one to recover a scaling law for the halocline depth consistent with equation (2) but also results in a scaling law for the adjustment time:

$$T \sim \frac{h}{W_{Ek}} \sim \frac{R^2}{K} \Rightarrow T \sim R^2 k^{-\frac{1}{3}} \left(\frac{\tau_0}{\rho_0 f} \right)^{-\frac{2}{3}}. \quad (3)$$

The power law dependence of T on the surface stress compares well with our eddy-resolving numerical simulations (Figure 3a, black).

Ocean models that do not resolve eddies and parameterize them assuming a constant eddy diffusivity would result in a time scale independent of mean surface stress—a gross misrepresentation of the gyre dynamics (Figure 3a, black). Instead, we see that an assumption that the eddy diffusivity $K \sim s^2$ proves to be most appropriate in simultaneously predicting scalings for both the gyre adjustment time scale T and the halocline depth h (Figure 3a).

3.3. Freshwater Release

We further illustrate important implications of the eddy effects by exploring the response of the Beaufort Gyre to a significant weakening of anticyclonic winds—a commonly occurring phenomena that leads to a release of the accumulated FWC. Here we perform the following numerical experiment. The gyre, initially at equilibrium under a wind stress ($\tau = 0.015 \text{ N m}^{-2}$), has its wind forcing decreased down to zero strength linearly over a time period of 5 years after which the winds remain off.

Over the 5 year period when the winds were decreasing, the FWC decreased only by a small fraction (Figure 3b). Indeed, for an effective release of FWC the weakening of anticyclonic winds has to persist longer than the gyre adjustment time.

We then consider the release of the freshwater and run model calculations where the anticyclonic winds were instantaneously decreased from steady value to zero to estimate an upper bound of the freshwater flux (FWF) out of the gyre. We find that the FWF decreases exponentially with time and its magnitude scales linearly with surface stress (Figure 3b, inset). Scaling suggests that $\text{FWF} \sim \text{FWC}/T$ and equations (2) and (3) together dictate that the FWF is directly related to the surface stress as

$$\text{FWF} \sim \frac{R^2 h}{T} \sim R^2 W_{Ek} \Rightarrow \text{FWF} \sim R \frac{\tau_0}{\rho_0 f}, \quad (4)$$

consistent with the model results.

The release of freshwater owes its existence entirely to the action of mesoscale eddies that slump the halocline previously deepened by winds. Nonetheless, because both FWC and T depend on eddy efficiency k in the same way (see equations (2) and (3)), a curious result arises: FWF is independent of the exact eddy parameterization scheme used (equation (4)). For example, if k increases, then the halocline depth and FWC would be smaller (equation (2)) but the gyre time scale would also shorten (equation (2)) such that their ratio or FWF remains the same. Thus, FWF scales in the same way as the Ekman pumping with its peak magnitude about 3 times larger than that supplied by the Ekman transport.

For the present-day gyre conditions, a release of the available FWC can provide a FWF of up to about $3000 \text{ km}^3 \text{ yr}^{-1}$ (Figure 3b, inset)—a flux comparable in magnitude with, for example, the FWF due to the entire sea ice transport from the Arctic Ocean [Haine *et al.*, 2015] or FWF represented by the Great Salinity Anomaly [Curry and Mauritzen, 2005]. Moreover, observations of the long-term intensification in surface stress [Giles *et al.*, 2012] imply that the potential FWF out of the gyre is also increasing.

4. Concluding Remarks

We have demonstrated that the Beaufort Gyre has an inherent time scale that is not associated with the time evolution of atmospheric winds or coastal water sources. Rather, it arises as a direct consequence of the

mesoscale eddy activity that is essential for sustaining the mean state of the gyre. Eddies fulfill an important task of exchanging the coastal water masses with the interior of the basin—a fundamental process that is fully capable of constraining the accumulation of freshwater due to Ekman pumping.

The presence of the gyre memory implies that a simple kinematic view, which assumes halocline deepening to be directly proportional to Ekman pumping, can represent conceptually accurate gyre dynamics only on short time scales. Thus, for example, the seasonal cycle is not significantly affected by eddies—a result that is consistent with other numerical studies [Davis *et al.*, 2014]. However, for interannual and decadal variations in atmospheric winds, eddies will substantially counteract the Ekman deepening/shallowing of the halocline and thus should be taken into account.

Our study suggests that continuing intensification of anticyclonic surface stress over the Beaufort Gyre will lead to the accumulation of FWC and to a significant shortening of the gyre response time scale. This would allow the gyre to potentially provide substantial freshwater fluxes to the shelves and neighboring basins, some of which may reach and influence deep convection regions in the North Atlantic.

The numerical model and theoretical considerations imply that due to eddy saturation effects, the Beaufort Gyre can hold a maximum of about 34 m of FWC. It is important to note that this bound is for the FWC associated only with the wind-driven halocline deepening and assumes that there are no changes in boundary water mass properties. Nonetheless, because of the current moderate forcing, the Beaufort Gyre is not near saturation and is expected to be highly sensitive to changes in surface stress. This is consistent with observations of its strong interannual and decadal wind-driven variability and suggests that care should be taken in accurately representing such high sensitivity in climate models.

Ocean circulation models that do not resolve eddies often implement a Gent-McWilliams eddy parameterization with a constant eddy diffusivity K [Gent and McWilliams, 1990]. This would result in a constant gyre adjustment time scale ($T \sim R^2/K$) and in the FWC being directly proportional to the strength of surface stress—a substantial misrepresentation of our idealized Beaufort Gyre dynamics. Due to the strong sensitivity of the mesoscale eddy transport to the slope of the halocline ($K \sim s^2$), the gyre adjustment becomes increasingly fast and the FWC bounded for strong surface stress forcing.

Finally, it is useful to point out a similarity between the dynamics of the Beaufort Gyre and the Antarctic Circumpolar Current (ACC) [Marshall and Radko, 2003; Hallberg and Gnanadesikan, 2006]. Both of these circulations rely fundamentally on the presence of mesoscale eddies that slump isopycnals to counteract their wind-driven steepening. However, the two circulations appear to be in different dynamical regimes. The ACC, driven by strong winds, is near the eddy saturation regime where its transport and isopycnal slope are only weakly sensitive to changes in winds [Farneti and Delworth, 2010; Tansley and Marshall, 2001; Hogg *et al.*, 2008; Abernathy *et al.*, 2011], whereas the Beaufort Gyre, as we demonstrated here, is currently highly sensitive to surface stress (Figure 3a).

Appendix A: Numerical Model Setup

The MITgcm version c65e (A. Adcroft *et al.*, MITgcm User Manual, 2015, http://mitgcm.org/public/r2_manual/latest/online_documents/manual.html) was used in our numerical simulations of the Beaufort Gyre. Horizontal resolution of 4 km with 34 vertical levels ranging between 10 m at the surface and 60 m at the bottom ensures that mesoscale eddies are sufficiently resolved (Rossby deformation radius is about 20 km). Horizontal diffusion of salinity and viscosity was set to zero, although the numeral discretization scheme does provide some nonzero dissipation (advection scheme 77 was used); a Smagorinsky-type horizontal viscosity with coefficient $A_h = 2.5$ was used for model stability. A quadratic bottom drag coefficient of 0.02 was used to dissipate momentum input from winds; free-slip lateral boundary conditions were used. For simplicity the imposed azimuthal surface stress is linearly increasing toward the coastal boundaries (i.e., $\tau \sim r$), providing a uniform Ekman pumping throughout the gyre (using other profiles did not change the conceptual view of the gyre dynamics and hence are not reported here). The vertical tracer diffusivity was set to $10^{-5} \text{ m}^2 \text{ s}^{-1}$, a value considered to be an upper bound for the Arctic Ocean. The f plane approximation was used with Coriolis parameter $f = 1.4 \times 10^{-4} \text{ s}^{-1}$, because the β effect has only a minor influence at the high latitudes of the Beaufort Gyre. A linear equation of state was used with only salinity contributing to the buoyancy (temperature has a minor impact for such strongly stratified flows at near-freezing temperatures). Boussinesq and hydrostatic approximations were used for simplicity as the area does not have strongly active deep

convection spots. Topography is azimuthally symmetric and represents a linearly increasing bathymetry from 300 m at the boundaries to 900 m over a horizontal distance of 100 km; the bottom is flat in the interior of the domain. No surface or bottom buoyancy fluxes were imposed; at the coastal boundaries (over two adjacent horizontal grid boxes) the vertical salinity distribution was strongly restored toward a representative profile with a time scale of 1 day. The model was integrated for 70 years to ensure equilibration.

Appendix B: Calculation of $\tilde{\psi}$

The residual stream function $\tilde{\psi}$ is computed in buoyancy coordinates using a z coordinate output of the MIT-gcm that was interpolated to isopycnal coordinates with 20 layers. Interface depths were obtained using a mass-conserving algorithm with a precision of one tenth of the vertical resolution to define layer thicknesses h ; the radial velocity u represents a vertically averaged value between adjacent interfaces. Thickness fluxes uh were averaged during the model calculations (“online”) using the “Layers” package as in *Abernathey et al.* [2011]. The residual stream function is then estimated as

$$\tilde{\psi}(r, b) = \int_0^{2\pi} \int_0^b \langle uh \rangle db' d\theta, \quad (B1)$$

where $\langle \rangle$ represent time averages over several eddy turnover periods (an alternative representation of ensemble averages) and b is the buoyancy. The stream function which is obtained in buoyancy coordinates is then interpolated onto height coordinates using a time mean relation between buoyancy and height: $\tilde{\psi}(z) = \tilde{\psi}(b(z))$. The time series of $\tilde{\psi}$ shown in Figure 3a represent a residual overturning mass transport which is calculated as a minimum value of $r\tilde{\psi}$ (negative values correspond to downwelling in the interior and upwelling at the coasts).

Acknowledgments

The authors acknowledge high-performance computing support from Yellowstone (ark:/85065/d7wd3xhc) provided by NCAR’s CIS Laboratory, sponsored by the NSF. GEM acknowledges the support from the Howland Postdoctoral Program Fund at WHOI. M.A.S. was supported by NSF grants PLR-1415489 and OCE-1232389. The manuscript benefited from discussions at the annual Forum for Arctic Modeling and Observing Synthesis (FAMOS) funded by the NSF OPP awards PLR-1313614 and PLR-1203720. The authors thank Andrey Proshutinsky for providing Figure 1 and for many valuable comments; Ryan Abernathey for providing a publicly available Layers package used in calculations of the residual circulation within the MITgcm; and Mary-Louise Timmermans, John Toole, Jiayan Yang, and John Marshall for discussions.

References

- Aagaard, K., and E. Carmack (1989), The role of sea ice and other fresh water in the Arctic circulation, *J. Geophys. Res.*, *94*(C10), 14,485–14,498.
- Abernathey, R., J. Marshall, and D. Ferreira (2011), The dependence of Southern Ocean meridional overturning on wind stress, *J. Phys. Oceanogr.*, *41*(12), 2261–2278.
- Aksenov, Y., V. V. Ivanov, A. Nurser, S. Bacon, I. V. Polyakov, A. C. Coward, A. C. Naveira-Garabato, and A. Beszczynska-Moeller (2011), The Arctic circumpolar boundary current, *J. Geophys. Res.*, *116*, C09017, doi:10.1029/2010JC006637.
- Allison, L. C., H. L. Johnson, and D. P. Marshall (2011), Spin-up and adjustment of the Antarctic Circumpolar Current and global pycnocline, *J. Mar. Res.*, *69*(2–3), 167–189.
- Belkin, I. M. (2004), Propagation of the “Great Salinity Anomaly” of the 1990’s around the northern North Atlantic, *Geophys. Res. Lett.*, *31*, L08306, doi:10.1029/2003GL019334.
- Belkin, I. M., S. Levitus, J. Antonov, and S.-A. Malmberg (1998), “Great Salinity Anomalies” in the North Atlantic, *Prog. Oceanogr.*, *41*(1), 1–68.
- Birner, T. (2010), Residual circulation and tropopause structure, *J. Atmos. Sci.*, *67*(8), 2582–2600.
- Boé, J., A. Hall, and X. Qu (2009), September sea-ice cover in the Arctic Ocean projected to vanish by 2100, *Nat. Geosci.*, *2*(5), 341–343.
- Bourgain, P., and J. C. Gascard (2012), The Atlantic and summer Pacific waters variability in the Arctic Ocean from 1997 to 2008, *Geophys. Res. Lett.*, *39*, L05603, doi:10.1029/2012GL051045.
- Cai, W.-J., et al. (2010), Decrease in the CO₂ uptake capacity in an ice-free arctic ocean basin, *Science*, *329*(5991), 556–559.
- Cole, S. T., M. L. Timmermans, J. M. Toole, R. A. Krishfield, and F. T. Thwaites (2014), Ekman veering, internal waves, and turbulence observed under Arctic sea ice, *J. Phys. Oceanogr.*, *44*(5), 1306–1328.
- Condron, A., P. Winsor, C. Hill, and D. Menemenlis (2009), Simulated response of the Arctic freshwater budget to extreme NAO wind forcing, *J. Clim.*, *22*(9), 2422–2437.
- Curry, R., and C. Mauritzen (2005), Dilution of the northern North Atlantic Ocean in recent decades, *Science*, *308*(5729), 1772–1774.
- Davis, P. E., C. Lique, and H. L. Johnson (2014), On the link between Arctic sea ice decline and the freshwater content of the Beaufort Gyre: Insights from a simple process model, *J. Clim.*, *27*(21), 8170–8184.
- Dickson, R., T. Osborn, J. Hurrell, J. Meincke, J. Blindheim, B. Adlandsvik, T. Vinje, G. Alekseev, and W. Maslowski (2000), The Arctic Ocean response to the North Atlantic Oscillation, *J. Clim.*, *13*(15), 2671–2696.
- Dickson, R. R., J. Meincke, S.-A. Malmberg, and A. J. Lee (1988), The “Great Salinity Anomaly” in the northern North Atlantic 1968–1982, *Prog. Oceanogr.*, *20*(2), 103–151.
- Dmitrenko, I., S. Kirillov, V. Ivanov, and R. Woodgate (2008), Mesoscale Atlantic water eddy off the Laptev Sea continental slope carries the signature of upstream interaction, *J. Geophys. Res.*, *113*, C07005, doi:10.1029/2007JC004491.
- Eisenman, I., and J. Wettlaufer (2009), Nonlinear threshold behavior during the loss of Arctic sea ice, *Proc. Natl. Acad. Sci.*, *106*(1), 28–32.
- Farneti, R., and T. L. Delworth (2010), The role of mesoscale eddies in the remote oceanic response to altered Southern Hemisphere winds, *J. Phys. Oceanogr.*, *40*(10), 2348–2354.
- Gent, P. R., and J. C. McWilliams (1990), Isopycnal mixing in ocean circulation models, *J. Phys. Oceanogr.*, *20*(1), 150–155.
- Giles, K. A., S. W. Laxon, A. L. Ridout, D. J. Wingham, and S. Bacon (2012), Western Arctic Ocean freshwater storage increased by wind-driven spin-up of the Beaufort Gyre, *Nat. Geosci.*, *5*(3), 194–197.
- Green, J. S. A. (1970), Transfer properties of the large-scale eddies and the general circulation of the atmosphere, *Q. J. R. Meteorol. Soc.*, *96*(408), 157–185.
- Haine, T. W., et al. (2015), Arctic freshwater export: Status, mechanisms, and prospects, *Global Planet. Change*, *125*, 13–35.
- Häkkinen, S. (1999), A simulation of thermohaline effects of a Great Salinity Anomaly, *J. Clim.*, *12*(6), 1781–1795.

- Hallberg, R., and A. Gnanadesikan (2006), The role of eddies in determining the structure and response of the wind-driven Southern Hemisphere overturning: Results from the modeling eddies in the Southern Ocean (MESO) project, *J. Phys. Oceanogr.*, *36*(12), 2232–2252.
- Held, I., and V. Larichev (1996), A scaling theory for horizontally homogeneous, baroclinically unstable flow on a beta plane, *J. Atmos. Sci.*, *53*(7), 946–952.
- Henning, C. C., and G. K. Vallis (2005), The effects of mesoscale eddies on the stratification and transport of an ocean with a circumpolar channel, *J. Phys. Oceanogr.*, *35*(5), 880–896.
- Hogg, A. M. C., M. P. Meredith, J. R. Blundell, and C. Wilson (2008), Eddy heat flux in the Southern Ocean: Response to variable wind forcing, *J. Clim.*, *21*(4), 608–620.
- Jansen, M. F., A. J. Adcroft, R. Hallberg, and I. M. Held (2015), Parameterization of eddy fluxes based on a mesoscale energy budget, *Ocean Modell.*, *92*, 28–41.
- Jones, D. C., T. Ito, and N. S. Lovenduski (2011), The transient response of the Southern Ocean pycnocline to changing atmospheric winds, *Geophys. Res. Lett.*, *38*, L15604, doi:10.1029/2011GL048145.
- Karsten, R., H. Jones, and J. Marshall (2002), The role of eddy transfer in setting the stratification and transport of a circumpolar current, *J. Phys. Oceanogr.*, *32*(1), 39–54.
- Karsten, R. H., and J. Marshall (2002), Constructing the residual circulation of the ACC from observations, *J. Phys. Oceanogr.*, *32*(12), 3315–3327.
- Krishfield, R. A., A. Proshutinsky, K. Tateyama, W. J. Williams, E. C. Carmack, F. A. McLaughlin, and M.-L. Timmermans (2014), Deterioration of perennial sea ice in the Beaufort Gyre from 2003 to 2012 and its impact on the oceanic freshwater cycle, *J. Geophys. Res. Oceans*, *119*, 1271–1305, doi:10.1002/2013JC008999.
- Li, W. K., F. A. McLaughlin, C. Lovejoy, and E. C. Carmack (2009), Smallest algae thrive as the Arctic Ocean freshens, *Science*, *326*(5952), 539–539.
- Lique, C., H. L. Johnson, and P. E. Davis (2015), On the interplay between the circulation in the surface and the intermediate layers of the Arctic Ocean, *J. Phys. Oceanogr.*, *45*(5), 1393–1409.
- Manley, T., and K. Hunkins (1985), Mesoscale eddies of the Arctic Ocean, *J. Geophys. Res.*, *90*(C3), 4911–4930.
- Manucharyan, G. E., and M.-L. Timmermans (2013), Generation and separation of mesoscale eddies from surface ocean fronts, *J. Phys. Oceanogr.*, *43*(12), 2545–2562.
- Marshall, J., and T. Radko (2003), Residual-mean solutions for the Antarctic Circumpolar Current and its associated overturning circulation, *J. Phys. Oceanogr.*, *33*(11), 2341–2354.
- Marshall, J., H. Jones, R. Karsten, and R. Wardle (2002), Can eddies set ocean stratification?, *J. Phys. Oceanogr.*, *32*(1), 26–38.
- Martin, T., M. Steele, and J. Zhang (2014), Seasonality and long-term trend of Arctic Ocean surface stress in a model, *J. Geophys. Res. Oceans*, *119*, 1723–1738, doi:10.1002/2013JC009425.
- McIntosh, P. C., and T. J. McDougall (1996), Isopycnal averaging and the residual mean circulation, *J. Phys. Oceanogr.*, *26*(8), 1655–1660.
- McLaughlin, F. A., and E. C. Carmack (2010), Deepening of the nutricline and chlorophyll maximum in the Canada Basin interior, 2003–2009, *Geophys. Res. Lett.*, *37*, L24602, doi:10.1029/2010GL045459.
- McPhee, M. G. (2013), Intensification of geostrophic currents in the Canada Basin, Arctic Ocean, *J. Clim.*, *26*(10), 3130–3138.
- Morison, J., R. Kwok, C. Peralta-Ferriz, M. Alkire, I. Rigor, R. Andersen, and M. Steele (2012), Changing Arctic Ocean freshwater pathways, *Nature*, *481*(7379), 66–70.
- Moritz, R. E., C. M. Bitz, and E. J. Steig (2002), Dynamics of recent climate change in the Arctic, *Science*, *297*(5586), 1497–1502.
- Nikurashin, M., and G. Vallis (2011), A theory of deep stratification and overturning circulation in the ocean, *J. Phys. Oceanogr.*, *41*(3), 485–502.
- Pedlosky, J. (1982), *Geophysical Fluid Dynamics*, 636 pp., Springer, Berlin, and New York.
- Peterson, B. J., R. M. Holmes, J. W. McClelland, C. J. Vörösmarty, R. B. Lammers, A. I. Shiklomanov, I. A. Shiklomanov, and S. Rahmstorf (2002), Increasing river discharge to the Arctic Ocean, *Science*, *298*(5601), 2171–2173.
- Pickart, R. S., M. A. Spall, and J. T. Mathis (2013), Dynamics of upwelling in the Alaskan Beaufort Sea and associated shelf–basin fluxes, *Deep Sea Res., Part I*, *76*, 35–51.
- Proshutinsky, A., R. Bourke, and F. McLaughlin (2002), The role of the Beaufort Gyre in Arctic climate variability: Seasonal to decadal climate scales, *Geophys. Res. Lett.*, *29*(23), 2100, doi:10.1029/2002GL015847.
- Proshutinsky, A., R. Krishfield, M.-L. Timmermans, J. Toole, E. Carmack, F. McLaughlin, W. J. Williams, S. Zimmermann, M. Itoh, and K. Shimada (2009), Beaufort Gyre freshwater reservoir: State and variability from observations, *J. Geophys. Res.*, *114*, C00A10, doi:10.1029/2008JC005104.
- Proshutinsky, A. Y., and M. A. Johnson (1997), Two circulation regimes of the wind-driven Arctic Ocean, *J. Geophys. Res.*, *102*(C6), 12,493–12,514.
- Rabe, B., M. Karcher, U. Schauer, J. M. Toole, R. A. Krishfield, S. Pisarev, F. Kauker, R. Gerdes, and T. Kikuchi (2011), An assessment of Arctic Ocean freshwater content changes from the 1990s to the 2006–2008 period, *Deep Sea Res., Part I*, *58*(2), 173–185.
- Rabe, B., M. Karcher, F. Kauker, U. Schauer, J. M. Toole, R. A. Krishfield, S. Pisarev, T. Kikuchi, and J. Su (2014), Arctic Ocean basin liquid freshwater storage trend 1992–2012, *Geophys. Res. Lett.*, *41*, 961–968, doi:10.1002/2013GL058121.
- Rudels, B. (2012), Arctic Ocean circulation and variability-advection and external forcing encounter constraints and local processes, *Ocean Sci.*, *8*, 261–286.
- Schweiger, A., R. Lindsay, J. Zhang, M. Steele, H. Stern, and R. Kwok (2011), Uncertainty in modeled Arctic sea ice volume, *J. Geophys. Res.*, *116*, C00D06, doi:10.1029/2011JC007084.
- Spall, M. A. (2013), On the circulation of Atlantic water in the Arctic Ocean, *J. Phys. Oceanogr.*, *43*(11), 2352–2371.
- Spall, M. A., R. S. Pickart, P. S. Fratantoni, and A. J. Plueddemann (2008), Western Arctic shelfbreak eddies: Formation and transport, *J. Phys. Oceanogr.*, *38*(8), 1644–1668.
- Stewart, K., and T. Haine (2013), Wind-driven Arctic freshwater anomalies, *Geophys. Res. Lett.*, *40*, 6196–6201, doi:10.1002/2013GL058247.
- Su, Z., A. L. Stewart, and A. F. Thompson (2014), An idealized model of Weddell Gyre export variability, *J. Phys. Oceanogr.*, *44*(6), 1671–1688.
- Tansley, C. E., and D. P. Marshall (2001), On the dynamics of wind-driven circumpolar currents, *J. Phys. Oceanogr.*, *31*(11), 3258–3273.
- Timmermans, M.-L., J. Toole, A. Proshutinsky, R. Krishfield, and A. Plueddemann (2008), Eddies in the Canada Basin, Arctic Ocean, observed from ice-tethered profilers, *J. Phys. Oceanogr.*, *38*(1), 133–145.
- Timmermans, M.-L., A. Proshutinsky, R. A. Krishfield, D. K. Perovich, J. Richter-Menge, T. Stanton, and J. M. Toole (2011), Surface freshening in the Arctic Ocean's Eurasian Basin: An apparent consequence of recent change in the wind-driven circulation, *J. Geophys. Res.*, *116*, C00D03, doi:10.1029/2011JC006975.

- Timmermans, M.-L., et al. (2014), Mechanisms of Pacific summer water variability in the Arctic's central Canada Basin, *J. Geophys. Res. Oceans*, *119*, 7523–7548, doi:10.1002/2014JC010273.
- Tremblay, J.-É., et al. (2011), Climate forcing multiplies biological productivity in the coastal Arctic Ocean, *Geophys. Res. Lett.*, *38*, L18604, doi:10.1029/2011GL048825.
- Vallis, G. K. (2006), *Atmospheric and Oceanic Fluid Dynamics: Fundamentals and Large-Scale Circulation*, Cambridge Univ. Press, Cambridge, U. K.
- Visbeck, M., J. Marshall, T. Haine, and M. Spall (1997), Specification of eddy transfer coefficients in coarse-resolution ocean circulation models, *J. Phys. Oceanogr.*, *27*(3), 381–402.
- Watanabe, E. (2011), Beaufort shelf break eddies and shelf-basin exchange of Pacific summer water in the western Arctic Ocean detected by satellite and modeling analyses, *J. Geophys. Res.*, *116*, C08034, doi:10.1029/2010JC006259.
- Watanabe, E. (2013), Linkages among halocline variability, shelf-basin interaction, and wind regimes in the Beaufort Sea demonstrated in pan-Arctic Ocean modeling framework, *Ocean Modell.*, *71*, 43–53.
- Zhang, R., and G. K. Vallis (2006), Impact of great salinity anomalies on the low-frequency variability of the North Atlantic climate, *J. Clim.*, *19*(3), 470–482.
- Zhao, M., M.-L. Timmermans, S. Cole, R. Krishfield, A. Proshutinsky, and J. Toole (2014), Characterizing the eddy field in the Arctic Ocean halocline, *J. Geophys. Res. Oceans*, *119*, 8800–8817, doi:10.1002/2014JC010488.